Available online at www.sciencedirect.com
SCIENCE DIRECT
Journal of Sound and Vibration 293 (2006) 667–679
JOURNAL OF SOUND AND VIBRATION
www.elsevier.com/locate/jsvi

A power flow method for evaluating vibration from underground railways

M.F.M. Hussein*, H.E.M. Hunt

Engineering Department, Cambridge University, Trumpington Street, Cambridge CB2 1PZ, UK

Accepted 26 August 2005
Available online 17 February 2006

Abstract

One of the major sources of ground-borne vibration is the running of trains in underground railway tunnels. Vibration is generated at the wheel–rail interface, from where it propagates through the tunnel and surrounding soil into nearby buildings. An understanding of the dynamic interfaces between track, tunnel and soil is essential before engineering solutions to the vibration problem can be found. A new method has been developed to evaluate the effectiveness of vibration countermeasures. The method is based on calculating the mean power flow from the tunnel, paying attention to that part of the power which radiates upwards to places where buildings' foundations are expected to be found. The mean power is calculated for an infinite train moving through the tunnel with a constant velocity. An elegant mathematical expression for the mean power flow is derived, which can be used with any underground-tunnel model. To evaluate the effect of vibration countermeasures and track properties on power flow, a comprehensive three-dimensional analytical model is used. It consists of Euler–Bernoulli beams to account for the rails and the track slab. These are coupled in the wavenumber–frequency domain to a thin shell representing the tunnel embedded within an infinite continuum, with a cylindrical cavity representing the surrounding soil.

1. Introduction

Underground railways are important for solving traffic congestion in densely populated cities. A serious disadvantage is the vibration generated by trains, which propagates from the wheel–rail interface through the tunnel and surrounding soil into nearby buildings. The resulting vibration and re-radiated noise causes annoyance to occupants particularly in the frequency range 0–200 Hz. Vibration at higher frequencies is generally attenuated rapidly with distance along the transmission path through the ground [1]. Many methods are used to decrease vibration levels in nearby structures [2,3]. One of the most effective methods is to isolate vibration at the source. A good example of source isolation is the use of floating-slab track as illustrated in Fig. 1. The principal components relevant to vibration modelling are the rails, the railpads and the floating slab. The floating slab is coupled via slab bearings to the tunnel wall which lines a cavity in the soil.

*Corresponding author. Tel.: +44 1223 765925: fax: +44 1223 332662.
E-mail addresses: mfmh2@cam.ac.uk (M.F.M. Hussein), hemh@cam.ac.uk (H.E.M. Hunt).

0022-460X/$ - see front matter © 2006 Elsevier Ltd. All rights reserved.
doi:10.1016/j.jsv.2005.12.012

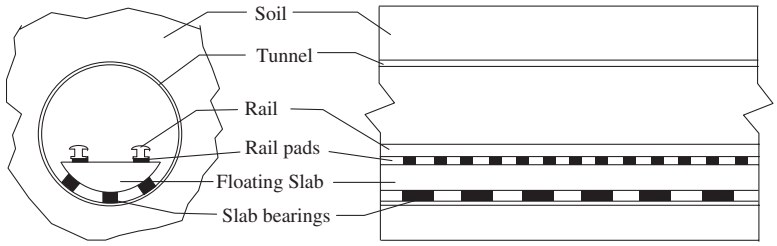

Fig. 1. Layout of an underground tunnel showing the different structural components (in this figure the floating slab is mounted on three lines of discrete slab bearings).

Existing models of underground railways use the displacement, velocity or acceleration power spectral density (PSD) calculated at some points in the track, tunnel or the ground as measures of vibration, see Ref. [4] for example. The PSD should be calculated in different directions and at many points to show the vibration environment at and away from the tunnel.

In this paper, a different measure of vibration is used to evaluate the effect of vibration countermeasures. This measure is based on the mean power flow from the tunnel, paying particular attention to the part of the power which radiates upwards to places where buildings' foundations are located. This measure has many advantages over the conventional approach, for instance:

- it provides a single measure of the vibration by calculating the power radiated upwards (the PSD at a single point is not representative for all places around the tunnel);
- it accounts for vibration in the vertical, horizontal and longitudinal directions at once (the PSD must be computed for each direction separately);
- the power-flow measure accounts for both the velocity and stress states around the tunnel.

The power-flow results, as will be seen later, depend on the transfer function between the rail input and the soil output. Therefore, the method can be applied to any model of surface or underground railways by using the appropriate transfer functions. In this paper, a model of a track in a deep-bored tunnel is used to investigate the power radiation, where no account is taken for any reflections. A detailed description of the method is given in Section 2. Sections 3 and 4 discuss the tunnel–soil model and the track model, respectively. Section 5 discusses the calculation procedure and finally, by means of a parametric survey, Section 6 provides some insight into the behaviour of the model and the effect of track properties on mean power flow.

2. Mean power flow due to an infinite moving train

A set of moving axles, infinite in number and with fixed axle spacing L, is used to model a train moving in an underground tunnel. As will be seen later in Section 2.3, the importance of the infinite-train model is that it causes the mean power flow to be independent of the longitudinal coordinates (in the tunnel direction) and hence reduces the three-dimensional problem to a two-dimensional one. The train model is shown in Fig. 2, where only unsprung masses are considered to give rise to dynamic forces on the track. The train moves with velocity v and due to a given sinusoidal rail roughness of wavelength λ_0, the rail experiences a harmonic excitation with angular frequency $\varpi = 2\pi\bar{f} = 2\pi v/\lambda_0$.

In this paper, correlated roughness on the two rails is assumed. Thus, the beam in Fig. 2 represents both rails of the track. The derivation in this section has been extended to uncorrelated roughness and is soon to be published [5]. This section is divided into three parts: firstly, an expression is found for the displacement at any point in the track or soil; secondly, the velocity and stress expressions are calculated; finally, these expressions are used to calculate the mean power flow.

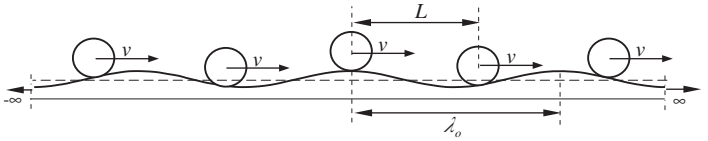

Fig. 2. Infinite number of masses move over a rail with roughness of wavelength λ_0 and magnitude Δ_0. Rail displacements are not shown.

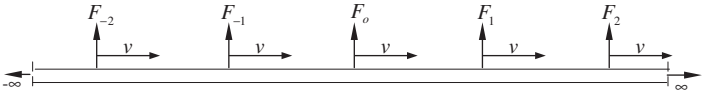

Fig. 3. Loading on the rail equivalent to the one in Fig. 2. $F_k = Ge^{i\varpi t}e^{ik\varpi L/v}$.

2.1. Displacements calculation of the track–tunnel–soil system

The loading in Fig. 2 is dynamically equivalent to a set of oscillating moving loads in the form $F_k = Ge^{i\varpi t}e^{ik\varpi L/v}$ as shown in Fig. 3. G is the magnitude of the applied force (constant for all axles), the phase difference between any adjacent loads is $\varpi L/v$, and the index k varies from $-\infty$ to ∞ . The load on the rail can be written in a continuous form as

$$F(x,t) = \sum_{k=-\infty}^{\infty} Ge^{i\varpi t}e^{ik\varpi L/v}\delta(x - vt - kL). \tag{1}$$

This force is transformed to the wavenumber–frequency domain ξ–ω using the double Fourier transform in time and space [6] to give

$$\tilde{F}(\xi,\omega) = 2\pi \sum_{k=-\infty}^{\infty} Ge^{i\xi nL}e^{ik\varpi L/v}\delta(\omega + \xi v - \varpi). \tag{2}$$

The displacement of the track or soil due to this loading is calculated using the convolution integral [6] as a multiplication in the ξ–ω domain. Hence,

$$\tilde{Y}(\xi,\omega) = 2\pi\,\tilde{H}(\xi,\omega) \sum_{k=-\infty}^{\infty} Ge^{i\xi kL}e^{ik\varpi L/v}\,\delta(\omega + \xi v - \varpi), \tag{3}$$

where $\tilde{H}(\xi,\omega)$ is the displacement frequency response function (FRF), i.e. the displacement of the measuring point (at track or soil) in the wavenumber–frequency domain for a unit force at the rail in the same domain. Transforming back to the time domain gives

$$\tilde{Y}(\xi,t) = \tilde{H}(\xi,\varpi - \xi v)Ge^{i(\varpi - \xi v)t} \sum_{k=-\infty}^{\infty} e^{ikL(\varpi/v - \xi)}. \tag{4}$$

The infinite sum of exponential functions can be written as an equivalent sum of delta functions [6] to give

$$\tilde{Y}(\xi,t) = \tilde{H}(\xi,\varpi - \xi v)Ge^{i(\varpi - \xi v)t}\frac{2\pi}{L}\sum_{k=-\infty}^{\infty}\delta\left(\xi - \varpi/v + \frac{2\pi k}{L}\right), \tag{5}$$

where k no longer gives the load index. Transforming back to the space domain and rearranging gives

$$y(x,t) = \sum_{k=-\infty}^{\infty} e^{i\xi_k x}e^{i\omega_k t}\left[\frac{G\tilde{H}(\xi_k,\omega_k)}{L}\right] \tag{6}$$

where

$$\xi_k = \frac{\varpi}{v} - \frac{2\pi k}{L} \quad \text{and} \quad \omega_k = \frac{2\pi k v}{L}.$$

This important result gives the displacement at any point in the track–soil system. It expresses the displacement as a sum of infinite convecting waves. Each wave is described with its angular frequency ω_k and wavenumber ξ_k, which is called the *wavenumber deficit*.

2.2. Velocity and stress calculations of the track–tunnel–soil system

Before writing the velocity and stress expressions, the magnitude of the force amplitude G in Eq. (6) is calculated by comparing the loading in Figs. 2 and 3 and writing the equilibrium of the mass located at $x = 0$ at time $t = 0$. This results in

$$G = \frac{M\Delta_0\varpi^2}{1 - y(0,0)_{G=1}M\varpi^2}, \tag{7}$$

where $y(0,0)_{G=1}$ is calculated from Eq. (6) by using the FRF of the rail $\tilde{H}(\xi,\omega)$ and substituting $G = 1$, M is the unsprung mass and Δ_0 is the roughness amplitude.

One can now calculate the velocity and stress at a point in soil by substituting the velocity and stress FRFs ($\tilde{V}(\xi_k,\omega_k)$ and $\tilde{\tau}(\xi_k,\omega_k)$) for the displacement FRF $\tilde{H}(\xi,\omega)$ in Eq. (6) to give

$$V(x,t) = \sum_{k=-\infty}^{\infty} e^{i\xi_k x}e^{i\omega_k t}\left[\frac{G\tilde{V}(\xi_k,\omega_k)}{L}\right], \tag{8}$$

$$\tau(x,t) = \sum_{k=-\infty}^{\infty} e^{i\xi_k x}e^{i\omega_k t}\left[\frac{G\tilde{\tau}(\xi_k,\omega_k)}{L}\right]. \tag{9}$$

2.3. Mean power flow calculation

Instantaneous local power flow is the product of local velocity and local stress. This forms the basis of the mean power flow method. The mean power flow can be calculated as

$$P(x) = \frac{v}{L}\int_{t=0}^{t=L/v} \mathrm{Re}(V(x,t))\mathrm{Re}(\tau(x,t))\,\mathrm{d}t. \tag{10}$$

Substituting Eqs. (8) and (9) into Eq. (10) after simplifications results in

$$P(x) = \frac{|G|^2}{2L^2}\sum_{k=-\infty}^{\infty} \mathrm{Re}[\tilde{V}(\xi_k,\omega_k)\tilde{\tau}^*(\xi_k,\omega_k)], \tag{11}$$

where $()^*$ denotes the conjugate of the complex quantity. The significance of this result is that it is independent of the longitudinal coordinate x. This confines the problem to the two-dimensional plane perpendicular to the longitudinal direction.

The infinite sum in Eq. (11) can be approximated as a finite sum performed over the region with large FRF response. This is made clear in Fig. 4, where the significant values of wavenumber deficit ξ_k are those that map onto regions of high $\tilde{V}(\xi,\omega)$ and $\tilde{\tau}(\xi_k,\omega_k)$.

3. Tunnel and soil model

A three-dimensional model for an underground tunnel and the surrounding soil is introduced by Forrest [7]. The tunnel wall is modelled as a thin cylindrical shell, while the soil around the tunnel is modelled using the elastic continuum theory as an infinite domain containing a cylindrical cavity as shown in Fig. 5.

The time-varying distributed stress applied to the tunnel wall is denoted $\tau(x,\theta,t)$, where x is the distance measured along the tunnel and θ is the angle measured around the circumference. This stress is transformed to the wavenumber domain using the Fourier transform along the direction x and due to circular periodicity, the θ dimension is decomposed into a discrete Fourier series with symmetrical and anti-symmetrical components

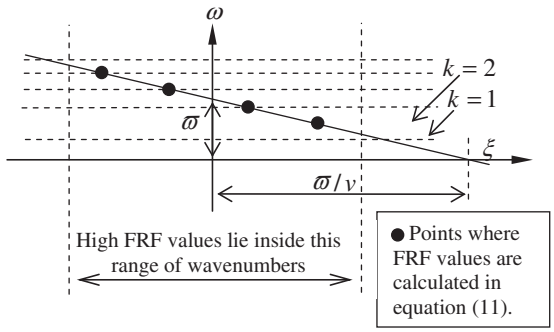

Fig. 4. Demonstration of the wavenumber region used in calculating Eq. (11). See Eq. (6) for the relationship between ξ_k and ω_k.

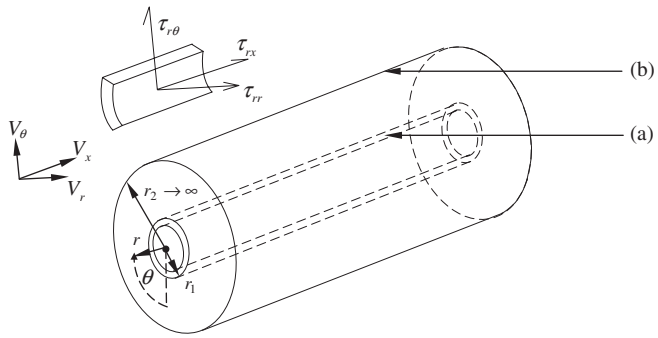

Fig. 5. Tunnel wall and soil models: (a) tunnel wall of outer radius r_1 modelled as a thin cylindrical shell of infinite length. (b) Surrounding soil modelled as an infinite domain with cylindrical cavity.

at the tunnel wall. The form of loading with symmetrical components with respect to θ can be written as

$$\tau(x,\theta,t) = \begin{bmatrix} \tilde{\tau}_{rx} \cos n\theta \\ \tilde{\tau}_{r\theta} \sin n\theta \\ \tilde{\tau}_{rr} \cos n\theta \end{bmatrix}_{r=r_t} e^{i(\omega t+\xi x)}, \tag{12}$$

where r_t is the internal radius of the tunnel. Note in Eq. (12) that $\tilde{\tau}_{r\theta} \sin n\theta$ is symmetrical rather than anti-symmetrical due to the sign convention for stress components as shown in Fig. 5. The soil velocities at radius r_0 measured from the tunnel centre, for the stress in Eq. (12), can be written as

$$V(x,\theta,t) = \begin{bmatrix} \tilde{V}_x \cos n\theta \\ \tilde{V}_\theta \sin n\theta \\ \tilde{V}_r \cos n\theta \end{bmatrix}_{r=r_0} e^{i(\omega t+\xi x)}. \tag{13}$$

To account for anti-symmetrical components (for instance, when torsional loading of the slab is considered), Eqs. (12) and (13) are used again, but every $\cos n\theta$ should be changed to $\sin n\theta$ and vice versa. When coupling a track to this model, the circumferential distribution of forces on the tunnel wall depends on the connectivity of the track. The model response to symmetrical and anti-symmetrical components can be found and the total response is calculated by adding the individual responses from Eq. (13). More details about the model are found in Refs. [5,7].

4. The track model

The track model consists of two rails and a main track slab modelled as Euler–Bernoulli beams [8]. The frequency range of interest of ground-borne vibration extends up to 200 Hz. This justifies using the

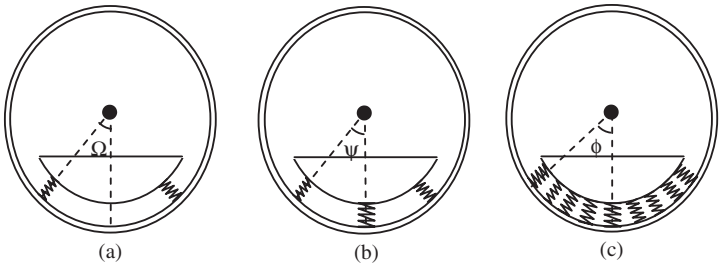

Fig. 6. Coupling of the slab to the tunnel–soil model via: (a) two lines, (b) three lines, and (c) uniform continuous support. Rails are not shown.

Euler–Bernoulli model, as the wavelengths of the propagating waves are much longer than the cross-sectional dimensions of the rails and slab. Rails transmit the load to the slab through railpads. Railpads are modelled as continuous resilient layers under the rails. The track is supported on the tunnel wall via slab bearings. Only bending of the slab is considered. The inclusion of torsional effects is straightforward [5], but not presented here. Three types of slab supports are considered, as shown in Fig. 6. The slab bearings in these models are continuous in the longitudinal direction and have both normal and shear stiffness. In reality, a floating slab is mounted on a thick layer of concrete in the base of the tunnel. Such a layer can be modelled as an extra "direct fastening" slab as demonstrated below. The inclusion of this layer is currently under development by the authors.

The main track slab is identified by its natural frequency. This is defined as the vertical cut-on frequency of the slab supported on a rigid tunnel via these slab bearings. The natural frequency of each slab [5] can be calculated from the relationships in Eqs. (14)–(16) for three cases (a), (b), and (c):

(a) *for two lines of support as in Fig.* 6(a):

$$f_n = \frac{1}{2\pi}\sqrt{\frac{k_n(2\cos^2\Omega + 2R\sin^2\Omega)}{m_s}}, \tag{14}$$

(b) *for three lines of support as in Fig.* 6(b):

$$f_n = \frac{1}{2\pi}\sqrt{\frac{k_n(2\cos^2\psi + 1 + 2R\sin^2\psi)}{m_s}}, \tag{15}$$

(c) *for uniform support as in Fig.* 6(c):

$$f_n = \frac{1}{2\pi}\sqrt{\frac{r_t k_n[\phi(1+R) + 0.5(1-R)\sin 2\phi]}{m_s}}, \tag{16}$$

where k_n is the slab-bearing normal stiffness, R is the ratio between the shear to the normal stiffness, i.e. $R = k_s/k_n$, k_s is the slab-bearing shear stiffness, m_s is the slab mass per unit length, r_t is the inner radius of the tunnel, and Ω, ψ, and ϕ are the angles of bearings distribution as shown in Fig. 6.

The main track slab is modelled in two ways, either "direct fastening" or "floating". "Direct fastening" (commonly known as "direct fixation") is modelled as case (c) (uniform support) by setting the slab-bearing stiffness to infinity. "Floating" track is modelled with any of the cases in Fig. 6 according to the distribution of slab bearings.

The track models are coupled to the tunnel–soil model in the wavenumber–frequency domain. This is done by considering equilibrium of forces and displacement at the interface between the slab bearings and the

tunnel wall. This allows for calculation of the velocity and stress FRFs at any given point (r, θ) in the soil for a unit input at the rails in the wavenumber–frequency domain.

5. Power calculation in the soil

The region of most interest for vibration in buildings is that part of the soil above the tunnel, since this is where foundations of buildings are located. Power radiated downwards is generally of no interest except perhaps in the case of rigid bedrock, not considered here. Hence, the mean power radiated upwards from the tunnel (see Fig. 7) is calculated and for the best design of track this value should be minimized. The power radiated through a circular sector with radius r_0 and bounded by the two angles θ_1 and θ_2 at an excitation frequency $\bar{f} = \varpi/(2\pi)$ can be calculated from the following expression (see Eq. (11)):

$$P(\theta_1, \theta_2) = \frac{|G|^2}{2L^2} \int_{\theta_1}^{\theta_2} \sum_{k=-\infty}^{\infty} \mathrm{Re}[\tilde{V}_x(\xi_k, \omega_k)\tilde{\tau}^*_{rx}(\xi_k, \omega_k) + \tilde{V}_\theta(\xi_k, \omega_k)\tilde{\tau}^*_{r\theta}(\xi_k, \omega_k) + \tilde{V}_r(\xi_k, \omega_k)\tilde{\tau}^*_{rr}(\xi_k, \omega_k)] r_0 \, \mathrm{d}\theta, \tag{17}$$

where all $\tilde{V}(\xi_k, \omega_k)$ and $\tilde{\tau}(\xi_k, \omega_k)$ are functions of θ. The three components in this expression take account of the power contributions from the longitudinal, tangential, and radial stresses, respectively. This equation provides an effective tool for checking the calculated expressions for stresses and displacements in the soil. The mean power calculated in this way for all closed boundaries that enclose the tunnel wall are identical, as there are no internal sources of power in the soil and no losses for the case of zero soil damping. At very low excitation frequency (near zero frequency), the mean input power at the tunnel wall and hence the mean power for a boundary enclosing the tunnel approach zero. This is because at such low frequency, the displacement is in phase with the induced force at the tunnel wall. This in turn makes the mean input power equal to zero. At higher excitation frequency, power is radiated away from the tunnel with much more radiation downwards than upwards, because the track is connected to the tunnel at its bottom. This has been investigated by the authors by producing colour plots of the power radiation around the tunnel for different excitation frequencies. However, these results are not presented here because this paper is concerned with integrating the mean power radiating upwards to present a single measure of the vibration rather than investigating vibration at different points around the tunnel.

The power radiated upwards can be evaluated using a semicircular boundary of radius r_0 as shown in Fig. 7. For the parameters given in Section 6, it is found that the evaluated mean power is effectively invariant for values of $r_0 \geqslant 10$ m (see Fig. 8) because there is no significant change of power flow across the horizontal part of the boundary. At semicircles near the tunnel wall, i.e. $r = 3$ m, it becomes necessary to account for power flow through the horizontal part of the boundary.

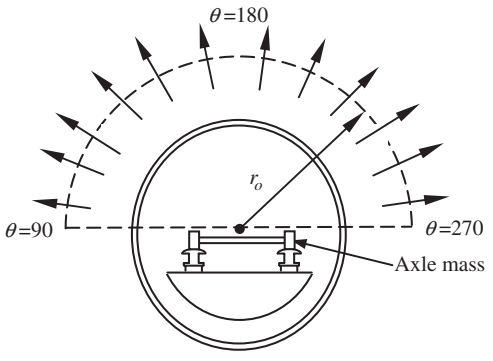

Fig. 7. Mean power flow radiated upward calculated at distance r_0 from the tunnel center due to infinite number of axles moving on the rails. Slab bearings are not shown in the diagram.

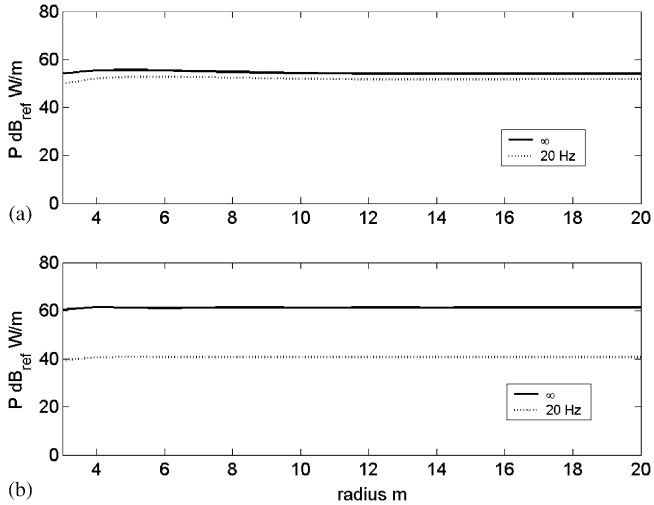

Fig. 8. Distance effect on the mean power flow radiated upward and calculated along semicircles with radii $3\,\text{m} \leqslant r_0 \leqslant 20\,\text{m}$ from the tunnel centre for a directly fixed slab (∞) and 20 Hz floating slab of uniform support with $\phi = 45^\circ$. The results are for train velocity 40 km/h and a roughness of excitations: (a) 30 Hz and (b) 100 Hz.

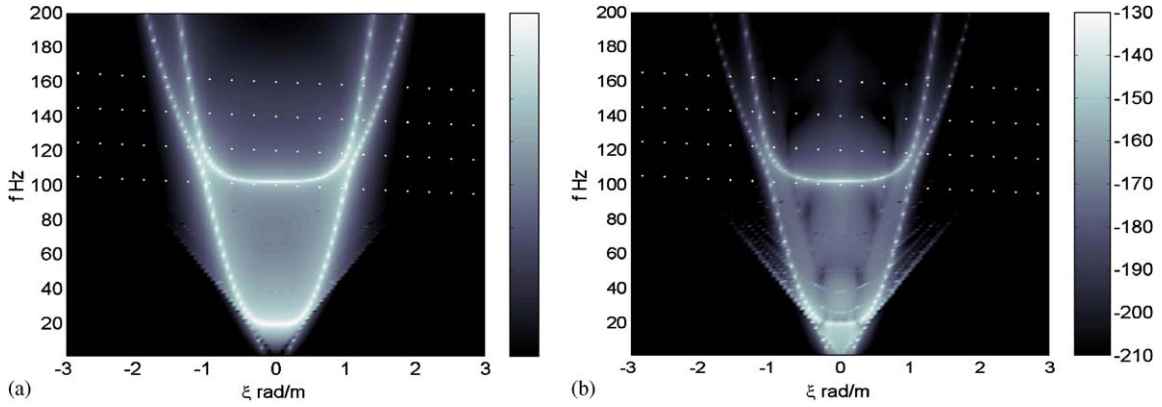

Fig. 9. (a) Tangential FRF velocity ($\text{d}B_{\text{ref}}$ m/s/N) at $r = 10\,\text{m}$, $\theta = 90^\circ$. (b) Radial FRF velocity ($\text{d}B_{\text{re}}$ 1 m/s/N) at $r = 10\,\text{m}$, $\theta = 180^\circ$. Results are for a unit input at the rail and the track is supported uniformly with $\phi = 45^\circ, f_n = 20\,\text{Hz}$. (No damping is included.) The four parallel dotted lines give $|v_k|$ in Eq. (17) for excitation frequencies $\bar{f} = 100$, 120, 140, and 160 Hz.

6. Effect of track properties on power flow

In this section, the general features of mean power flow from an underground tunnel are investigated. Hence, the effects of changing parameters such as unsprung mass, bending stiffness of rail and slab, stiffness of railpads and slab bearings, and the distribution of slab bearings are studied.

Figs. 9(a, b) show the magnitude of the tangential and radial velocity FRFs at $\theta = 90^\circ$ and 180°, respectively, at radius $r_0 = 10\,\text{m}$ for a 20 Hz slab on uniform support. The distinct white curves indicate high values of the velocity FRF and the two continuous curves are clearly visible. These correspond to the *dispersion curves* for a track on a rigid foundation as confirmed later (Fig. 12(b)). The dispersion curve is used to determine the wavenumber of free wave propagation at a given frequency. It can be seen from the two dispersion curves that cut-on frequencies occur at 20 Hz, where the slab resonates, and at 100 Hz, where the rails resonate.

Fig. 10(a) shows the upwards mean power flow, calculated at $r_0 = 10\,\text{m}$ and integrated over a half-circle from $\theta = 90^\circ$ to 270°. The four curves are for progressively more resilient slab support, i.e. for ∞, 40, 20, and

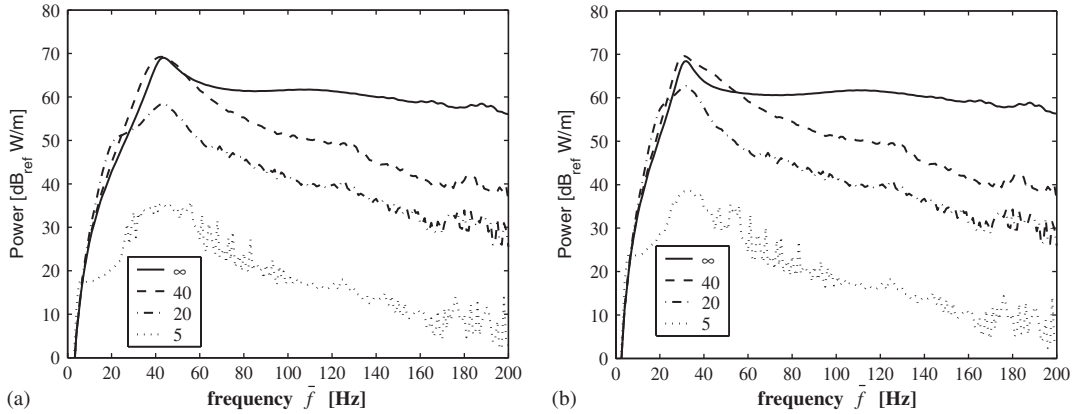

Fig. 10. (a) Mean power flow radiated upwards, for different slab-bearings stiffness. (b) Effect of doubling the unsprung mass at (a).

5 Hz slabs. The slab is uniformly supported with $\phi = 45^\circ$ as in Fig. 6(c). The power results in this figure are calculated at 1 Hz frequency intervals (from 1 to 200 Hz) by averaging the results within each 1 Hz band (0.5 Hz on either side). In each band the results are calculated for every 0.1 Hz increment.

Averaging is used to smooth the curves which otherwise fluctuate severely. This is on account of discrete sampling of the FRFs (see Figs. 4 and 9). Fluctuations are attributed to the high levels of FRFs at points along the dispersion curves. At a given excitation frequency, some values of $V(\xi_k, \omega_k)$ lie on or near the track's dispersion curves, which leads to a peak. At another frequency, none of the values of $V(\xi_k, \omega_k)$ lie on or near the track's dispersion curves, which leads to a trough. Introducing some damping in the track also leads to curve smoothing. This is because damping attenuates the high levels of FRF at dispersion curves of the track.

In Fig. 10(a), the most distinguishable peaks for all curves occur at 42 Hz. This frequency is the wheel–track resonance frequency in which the wheels and axle resonate on the track. The parameters which control this peak are described in the next section. Another peak occurs at the cut-on frequency of the slab. For 40 Hz floating slab, this happens to coincide closely with the wheel resonance frequency.

6.1. Model parameters

Parameters used for the train, track, tunnel, and soil [7] are given below. The parameters of the train and track are typical. The tunnel parameters are those for a concrete tunnel, while the soil parameters are average values estimated for Oxford Clay. The effects of changing the parameters of the track are discussed in the next sub-sections.

Train: unsprung axle mass $M_a = 1000\,\text{kg}$, velocity $v = 40\,\text{km/h}$, axle spacing $L = 20\,\text{m}$.

Track: rail bending stiffness $\text{EI}_r = 5\,\text{MPa m}^4$, rail mass $m_r = 50\,\text{kg/m}$, slab bending stiffness $\text{EI}_s = 1430\,\text{MPa m}^4$, slab mass $m_s = 3500\,\text{kg/m}$, railpad stiffness $k_r = 20\,\text{MN/m}^2$, railpad loss factor $\eta_{kr'} = 0.3$, slab-bearing loss factor $\eta_{ks} = 0.5$, slab-bearing shear to normal stiffness ratio $R = 1$ for direct fixation, i.e. ∞ Hz and 0.5 for other slabs (i.e. 40, 20, and 5 Hz).

Tunnel: mean radius $r_a = 3.0\,\text{m}$, thickness $h = 0.25\,\text{m}$, modulus of elasticity $E_t = 50\,\text{GPa}$, Poisson's ratio $\upsilon_t = 0.3$, density $\rho_t = 2500\,\text{kg/m}^3$, and no damping.

Soil: compression wave speed $c_1 = 944\,\text{m/s}$, shear wave speed $c_2 = 309\,\text{m/s}$, Poisson's ratio $\upsilon_s = 0.44$, and no damping.

6.2. Effect of unsprung mass on power flow (wheel–track resonance)

The wheel–track system at resonance can be described as a single-degree-of-freedom system with a mass equal to the unsprung mass of the train plus that part of the rail which moves up and down with the wheel and a stiffness equal to the track stiffness underneath the wheels. A closed-form equation for calculating the resonance frequency is derived from the resonance of a mass coupled to a beam on a Winkler foundation and

can be written as

$$(m_b\omega^2 - k_f)^3 + \frac{M_a^4}{64\mathrm{EI}_b}\omega^8 = 0, \tag{18}$$

where m_b is the beam mass per unit length, EI_b is the beam bending stiffness, k_f is the foundation stiffness, and M_a is the coupled mass. One can prove Eq. (18), using the response of a beam on an elastic foundation under a unit concentrated harmonic load with angular frequency ϖ applied at $x = 0$ and given by Eq. (19), see Ref. [7] for example:

$$y_b(x,t) = \frac{1}{4\alpha^3\mathrm{EI}_b}(\mathrm{e}^{\alpha|x|} + \mathrm{i}\mathrm{e}^{\mathrm{i}\alpha|x|})\mathrm{e}^{\mathrm{i}\varpi t} \quad \text{with } \alpha^4 = \frac{m_b\varpi^2 - k_f}{\mathrm{EI}_b}. \tag{19}$$

The value of α in Eq. (19) should be chosen to be with a negative real value if α^4 is positive, while it should be chosen in the third quadrant if α^4 is negative. If a mass M_a is coupled to the beam at $x = 0$ and excited by a unit harmonic load with angular frequency ϖ, the mass displacement is described by

$$y_{M_a}(t) = \frac{1}{1/y_b(0,0) - M_a\varpi^2}\mathrm{e}^{\mathrm{i}\varpi t}. \tag{20}$$

From Eq. (20), a resonance occurs when $1/y_b(0,0) - M_a\varpi^2$, substituting for $y_b(0,0)$ from Eq. (19) and simplifying results in Eq. (18).

Using the rail parameters from Section 6.1, the wheel–track resonance is found to be 42 Hz, which matches with the results in Fig. 10(a). Doubling the unsprung mass to $M_a = 2000$ kg leads to the results in Fig. 10(b). Using Eq. (18) leads to wheel–track resonance equal to 31 Hz, which matches the results in Fig. 10(b).

6.3. Effect of slab bearings on power flow

Slab bearings isolate the track from the tunnel-transforming part of the wheel input into slab vibration and thus decreasing forces at the tunnel wall. For slabs with low natural frequencies as calculated by Eqs. (14)–(16), slab bearings decouple the track from the tunnel. This enables the soil FRFs to be calculated in a different way. Firstly, forces on the tunnel wall are calculated assuming a rigid tunnel. These forces are then used as input to the tunnel–soil model to calculate the soil FRFs. Fig. 12(a) shows the dispersion curves for a track on rigid foundation with infinite stiffness slab bearings. Only one mode can propagate along rails with a cut-on frequency at 100 Hz. Introducing slab bearings (20 Hz natural frequency of slab) leads to another mode. Crossover of modes occurs between 100 and 120 Hz. This can be seen by comparing Figs. 12(a) and (b). Such a phenomenon occurs in other waveguide solutions, see Ref. [9] for example.

6.4. Effect of railpads stiffness on power flow

Fig. 11 shows the effect of changing the railpad stiffness from 20 to 2 MN/m^2. The mean power insertion gain (PFIG) [10] is used and defined as

$$\mathrm{PFIG} = 10\log_{10}\left(\frac{P_{\mathrm{after}}}{P_{\mathrm{before}}}\right), \tag{21}$$

where P_{before} and P_{after} are the mean power radiated upwards before and after changing some of the track properties, respectively. In Fig. 11, P_{before} is calculated for four tracks with the same railpad stiffness (20 MN/m^2), but with different slab bearings stiffness. P_{after} is calculated for the same four tracks with different stiffness of the railpads (2 MN/m^2). It can be seen that changing the stiffness of railpad leads to a change in the wheel–track resonance frequency (from 42 to 24 Hz) and decreases the power radiation at high frequencies (above 70 Hz) by an average of 8 dB.

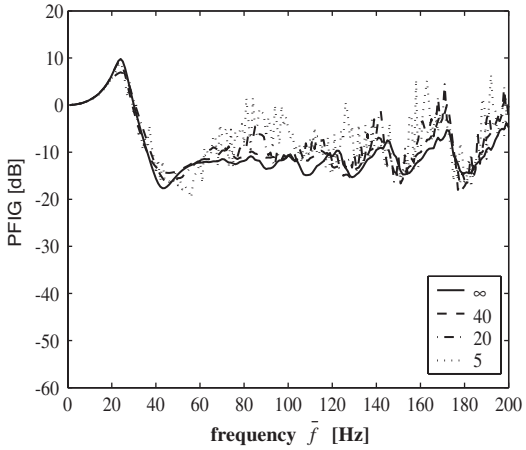

Fig. 11. Insertion gain due to changing the railpad stiffness from 20 to 2 MN/m^2.

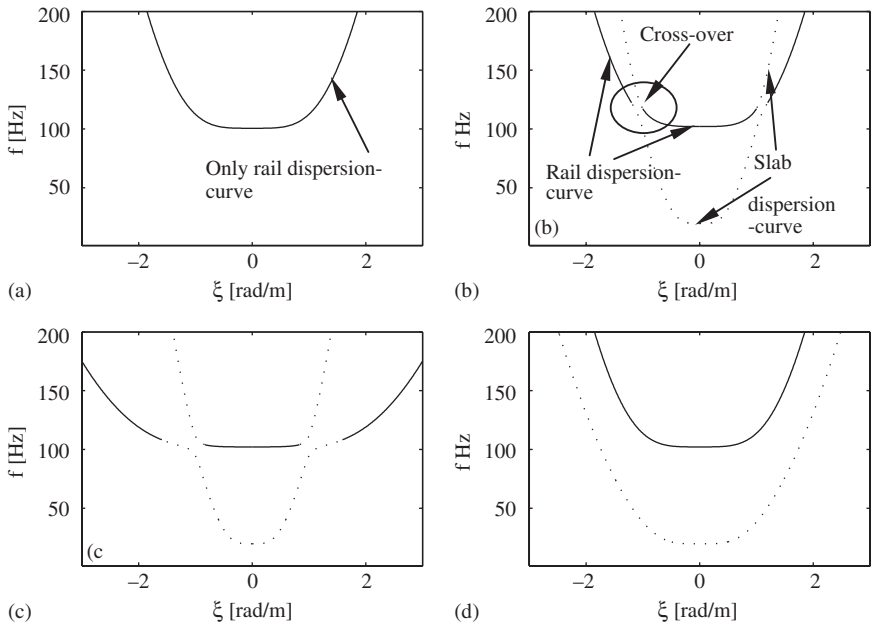

Fig. 12. Dispersion curves of a track (rails (—) and slab (· · · · · ·)) on rigid foundation. (a) ∞ Hz slab. (b) 20 Hz slab. (c) Same parameters as used in (b), but with 1/10 bending stiffness of rail. (d) Same parameters as used in (b), but with 1/10 bending stiffness of slab.

6.5. *Effect of bending stiffness of rail and slab on power flow*

According to Eq. (18), changing the bending stiffness of the rail affects the wheel–track resonance frequency because it changes the track stiffness under the wheel. Comparing Figs. 12(b) and (c) reveals that another effect of decreasing the rail bending stiffness is the broadening of the rail dispersion curve. The same effect can be seen for the slab dispersion curve by changing the slab bending stiffness (compare Fig. 12(d) with (b)). Investigation of the coupled tunnel–soil model shows that it strongly attenuates vibration at large wavenumbers. This means vibration can be attenuated by broadening the track dispersion curves, so that they occur at high wavenumbers and thus are attenuated by the tunnel–soil model. Figs. 13(a) and (b) show the PFIG by decreasing the bending stiffness of the rail and the slab, respectively, to one-tenth of their original values.

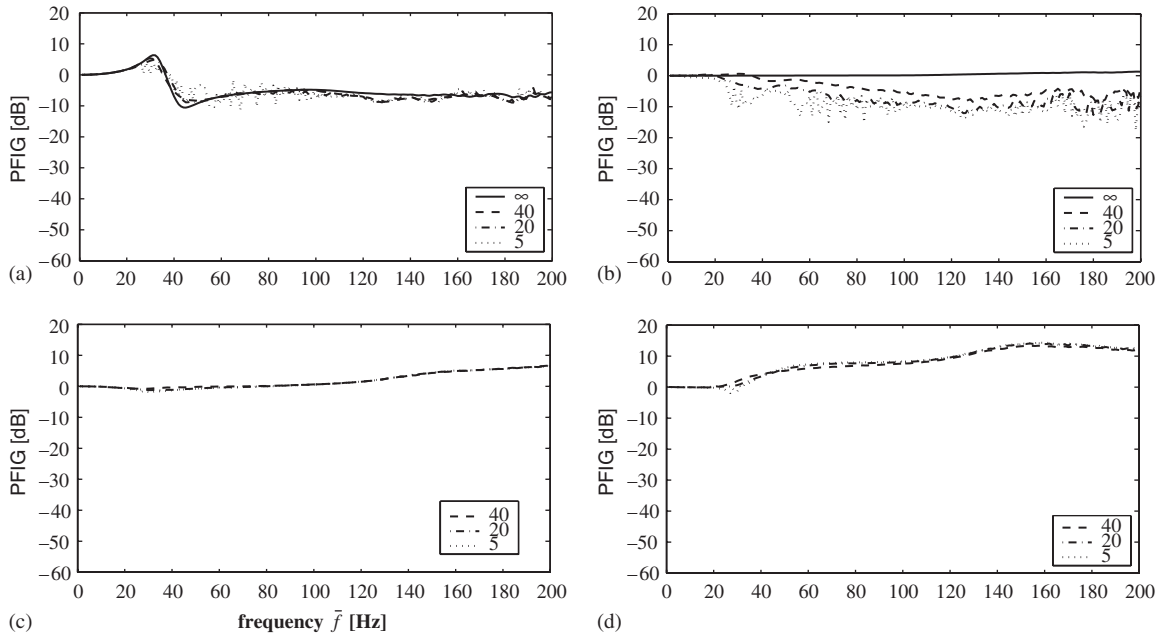

Fig. 13. Insertion gain due to (a) changing the bending stiffness of rail from 5 to 0.5 MPa m^4. (b) Changing the bending stiffness of slab from 1430 to 143 MPa m^4. (c) Replacing the uniform slab bearings by three lines of slab bearing ($\psi = 45°$). (d) Replacing the uniform slab bearings by two lines of slab bearing ($\Omega = 45°$).

6.6. *Effect of distribution of slab bearings on power flow*

Figs. 13(c) and (d) show examples of controlling the power radiated upwards. Changing the distribution of the slab-bearings controls the azimuthal distribution of the load on the tunnel. In these cases, the mean power flow is increased up to 14 dB by supporting the slab via three lines and two lines with respect to the uniform support. This is because the tunnel is less constrained by using a discrete track support compared to the uniform track support, leading to more vibration. An important conclusion is drawn from Figs. 13(c) and (d) that the details of the track support (the distribution of slab bearings) have a significant effect on the power flow and consequently on the vibration propagating from underground railways. Therefore, more attention should be paid in modelling to the support distribution, especially for prediction models [11] of vibration from underground railways.

7. Conclusions

A new method based on power flow calculations is presented to evaluate the performance of vibration countermeasures for underground tunnels. An expression of the power radiation is derived for an infinite train moving through the tunnel. A three-dimensional model of a track coupled to a tunnel in the ground is used to investigate the upward mean power from the tunnel. The track properties along with the tunnel–soil–track interaction play important roles in controlling the radiated power. The method is used to investigate the effect of unsprung mass, railpads, slab bearings, railpads, and bending stiffness of rail and slab.

Acknowledgement

The authors would like to thank Cambridge Overseas Trust COT and London Underground Limited LUL for their support of this project.

References

[1] C.J.C. Jones, J.R. Block, Prediction of ground vibration from freight trains, *Journal of Sound and Vibration* 193 (1) (1996) 205–213.
[2] P.J. Remington, L.G. Kurzweil, D.A. Towers, in: P.M. Nelson (Ed.), *Low-Frequency Noise and Vibration from Trains. Chapter 16 from Transportation Noise Reference Book*, Butterworth & Co. Ltd., London, 1987.
[3] G.P. Wilson, H.J. Saurenman, J.T. Nelson, Control of ground-borne noise and vibration, *Journal of Sound and Vibration* 87 (2) (1983) 339–350.
[4] M.F.M. Hussein, H.E.M. Hunt, An insertion loss model for evaluating the performance of floating-slab track for underground railway tunnels. *Proceedings of the Tenth International Congress on Sound and Vibration* 2003, pp. 419–426.
[5] M.F.M. Hussein, Vibration from Underground Railways, PhD Dissertation, Cambridge University, Cambridge, 2004.
[6] D.E. Newland, *An Introduction to Random Vibrations, Spectral & Wavelet Analysis*, Longman Singapore Publishers Ltd., New York, 1975.
[7] J.A. Forrest, Modelling of Ground Vibration from Underground Railways, PhD Dissertation, Cambridge University, Cambridge, 1999.
[8] S. Timoshenko, D.H. Young, W. Weaver, *Vibration Problems in Engineering*, fourth ed., New York, 1974.
[9] A.E. Armenakas, D.C. Gazis, G. Herrmann, *Free Vibrations of Circular Cylindrical Shells*, first ed., Pergamon Press Inc., Oxford, 1969.
[10] J.P. Talbot, H.E.M. Hunt, On the performance of base-isolated buildings, *Building Acoustics* 7 (2) (2000) 163–178.
[11] D. Clouteau, M. Arnst, T.M. Al-Hussaini, G. Degrande, Freefield vibrations due to dynamic loading on a tunnel embedded in a stratified medium, *Journal of Sound and Vibration* 283 (2005) 173–199.